HHS Public Access

Author manuscript

Neuron Behav Data Anal Theory. Author manuscript; available in PMC 2023 May 12.

Published in final edited form as:

Neuron Behav Data Anal Theory. 2022 ; 1: . doi:10.51628/001c.38960.

Golden rhythms as a theoretical framework for cross-frequency organization

Mark A. Kramer[1,2]

[1]Department of Mathematics and Statistics, Boston University

[2]Center for Systems Neuroscience, Boston University

Abstract

While brain rhythms appear fundamental to brain function, why brain rhythms consistently organize into the small set of discrete frequency bands observed remains unknown. Here we propose that rhythms separated by factors of the golden ratio $(\phi = (1 + \sqrt{5})/2))$ optimally support segregation and cross-frequency integration of information transmission in the brain. Organized by the golden ratio, pairs of transient rhythms support multiplexing by reducing interference between separate communication channels, and triplets of transient rhythms support integration of signals to establish a hierarchy of cross-frequency interactions. We illustrate this framework in simulation and apply this framework to propose four hypotheses.

Keywords

oscillations; cross-frequency coupling; multiplexing; neural communication system

1 | INTRODUCTION

The brain is organized into a hierarchy of functionally specialized regions, which selectively coordinate during behavior [1, 2, 3, 4] and rest [5, 6, 7]. Effective function relies on dynamic coordination between brain regions, in response to a changing environment, on an essentially fixed and limited anatomical substrate [8, 9, 10, 11]. Through these anatomical connections multiplexing occurs: multiple signals that combine for transmission through a single communication channel must then be differentiated at a downstream target location [12, 13]. How information – communicated via coordinated transmission of spiking activity [14] – dynamically routes through the brain's complex, distributed, hierarchical network remains unknown [15].

Brain rhythms – approximately periodic fluctuations in neural population activity – have been proposed to control the flow of information within the brain network [12, 16, 17, 18, 19, 20] and proposed as the core of cognition [21, 22, 23, 24]. Through periodic modulations in neuronal excitability, rhythms may support flexible and selective communication, allowing exchange of information through coordination of phase at rhythms

Correspondence: Mark A. Kramer, Department of Mathematics and Statistics, Boston University, Boston, MA, 02115, USA, mak@bu.edu.

of the same frequency (e.g., coherence [16, 19, 25, 26, 27]) and different frequencies (e.g., phase-amplitude coupling [18, 28, 29] or n:m phase locking [30, 31, 32]). Recent evidence shows that neural oscillations appear as transient, isolated events [33, 34]; how such transient oscillations route information through neural networks remains unclear [35].

Significant evidence supports the organization of brain rhythms into a small set of discrete frequency bands (e.g., theta [4–8 Hz], alpha [8–12 Hz], beta [12–30 Hz], gamma [30–80 Hz]) [36, 37]. Consistent frequency bands appear across mammalian species (mouse, rat, cat, macaque, and humans [38]) and in some cases the biological mechanisms that pace a rhythm are well-established (e.g., the decay time of inhibitory post-synaptic potentials sets the timescale for the gamma rhythm [39]). Why brain rhythms organize into discrete bands, and whether these rhythms are fixed by the brain's biology or organized to optimally support brain communication, remains unclear. For example, an alternative organization of the brain's rhythms (e.g., into a larger set of different frequency bands) may better support communication but remain inaccessible given the biological mechanisms available to pace brain rhythms.

While much evidence supports the existence of brain rhythms and their importance to brain function, few theories explain their arrangement. Different factors have been proposed for the spacing between the center frequencies of neighboring bands: Euler's number ($e \approx 2.718$) [40], the integer 2 [41], or the golden ratio ($\phi \approx 1.618$) [42]. Existing theory shows that irrational factors (e.g., e and ϕ) minimize interference between frequency bands, in support of separate rhythmic communication channels for multiplexing information in the brain [43, 44, 45]. However, if separate rhythmic channels communicate different information, and the organization of brain rhythms prevents interference, how a target location coordinates information across these rhythms is unclear. For example, how in theory a neural population integrates top-down and bottom-up input communicated in separate rhythmic channels (lower [<40 Hz] and higher [>40 Hz] frequency ranges, respectively [25, 26, 46, 47, 48]) remains unclear. We propose a solution to this problem: addition of a third rhythm. Motivated by an existing mathematical theory [43, 44, 45], we show that effective communication among three rhythms is optimal for rhythms arranged according to the golden ratio.

In what follows, we show that golden rhythms – rhythms organized by the golden ratio – are the optimal choice to integrate information among separate rhythmic communication channels. We propose that brain rhythms organize in the discrete frequency bands observed, with the specific spacing observed, to optimize segregation and integration of information transmission in the brain.

2 | METHODS

All simulations and analysis methods to reproduce the manuscript results and figures are available at https://github.com/Mark-Kramer/Golden-Framework.

2.1 | Damped harmonic oscillator model

As a simple model of rhythmic neural population activity (e.g., observed in the local field potential (LFP) or magneto/electroencephalogram (M/EEG)) we implement a network of coupled damped harmonic oscillators [49]. We choose the damped harmonic oscillator for three reasons. First, a harmonic oscillator (e.g., a spring) mimics the restorative mechanisms governing displacements about a stable equilibrium in neural dynamics (e.g., excitation followed by inhibition in the gamma rhythm [39, 50], depolarization followed by hyperpolarization – and vice versa – in bursting rhythms [51]). Second, brain rhythms are transient [33, 34]. In the model, damping (e.g., friction) produces transient oscillations that decay to a stable equilibrium. Third, the damped harmonic oscillator driven by noise is equivalent to an autoregressive model of order two (AR(2), see Appendix A). The AR(2) model simulates stochastic brain oscillations [52], consistent with the concept of a neural population with resonant frequency driven by random inputs.

We simulate an 8-node network of damped, driven harmonic oscillators. We model the activity x_k at node k as,

$$\ddot{x}_k + 2\beta\dot{x}_k + \omega_k^2 x_k = (\bar{g}_C + \bar{g}_S \cos\omega_S t) \sum_{j \neq k} x_j, \tag{1}$$

where β is the damping constant, and $\omega_k = 2\pi f_k$ is the natural frequency of node k. The activity x_j summed from all other nodes ($j \neq k$) drives node k. We modulate this drive by a gain function with two terms: a constant gain $\bar{g}_C$ and a sinusoidal gain with amplitude $\bar{g}_S$ and frequency $\omega_S = 2\pi f_S$. To include noise in the dynamics, we represent the second order differential equation in Equation (1) as two first order differential equations for the position and velocity of the oscillator. We add to the position dynamics a noise term, normally distributed with mean zero and standard deviation equal to the average standard deviation of the evoked response at all oscillators simulated without noise, excluding the perturbed oscillator from the average. In this way, we add meaningful noise of the same magnitude to all oscillators. We numerically simulate the model with noise using the Euler-Maruyama method. To examine the impact of different noise levels, we multiply the noise term by factors {0, 0.5, 1.0, 1.5, 2.0}. For each noise level, we repeat the simulation 100 times with random noise instantiations.

3 | RESULTS

In what follows, we propose that brain rhythms organized according to the golden ratio produce triplets of rhythms that establish a hierarchy of cross-frequency coupling. We conclude with four hypotheses deduced from this framework and testable in experiments.

3.1 | Rhythms organized by the golden ratio support selective cross-frequency coupling

In the case of weakly-connected oscillatory populations, whether the populations interact or not depends on their frequency ratios [43, 44, 45]; rational frequency ratios support interactions, while irrational frequency ratios do not. Motivated by this theory, we consider a network of interacting, rhythmic neural populations (Figure 1). We model each population as a damped harmonic oscillator, with each oscillator assigned a natural frequency f_k. To

couple the populations, we drive each oscillator with the summed activity of all other oscillators (i.e., the connectivity is all-to-all). We modulate this drive by a gain function (g) with constant ($\bar{g}_C$) and sinusoidal (amplitude $\bar{g}_S$, frequency f_S) terms: $g = \bar{g}_C + \bar{g}_S \cos(2\pi f_S t)$; see Methods. Analysis of this coupled oscillator system reveals resonance (i.e., a large amplitude response) at a target oscillator in two cases. To describe these cases, we denote the frequency of a target oscillator as f_T and the frequency of a driver oscillator as f_D. A large amplitude (resonant) response occurs at the target oscillator in the following cases,

constant gain modulation:

$$0 = f_T - f_D \tag{2}$$

sinusoidal gain modulation:

$$f_S = f_T - f_D \tag{3a}$$

$$f_S = f_D - f_T \tag{3b}$$

$$f_S = f_D + f_T \tag{3c}$$

The first case (Equation 2) corresponds to the standard result for a damped target oscillator driven by sinusoidal input; when the sinusoidal driver frequency f_D matches the natural frequency of the target f_T, the response amplitude at the target is largest (e.g., see Chapter 5 of [53]). The next three cases (Equation 3) correspond to a damped target oscillator driven by sinusoidal input modulated by sinusoidal gain. If the gain frequency f_S equals the sum or difference of the target and driver frequencies, then the response amplitude at the target is largest (see Appendix B). We note that the first case corresponds to within-frequency coupling (i.e., the driver and target have the same frequency) while the next three cases correspond to cross-frequency coupling (i.e., the driver and target have different frequencies). We also note that, in this model, we assume an oscillator responds to an input by exhibiting a large amplitude response; in this way, we consider the oscillation amplitude as encoding information, consistent with notion of information encoded in firing rate modulations [54].

The results in Equations (2, 3) hold for any choice of driver, target, and gain frequencies without additional restrictions. We now apply an additional restriction, and consider the damped harmonic oscillator network with oscillator and gain frequencies f_k satisfying,

$$f_k = f_0 c^k, \tag{4}$$

where $f_0 > 0$ determines the frequency at $k = 0$. As discussed above, candidate values for c deduced from *in vivo* observations include Euler's number ($e \approx 2.718$) [40], the integer 2 [41], or the golden ratio ($\phi \approx 1.618$) [42]. Then, given the set of three neighboring frequencies $\{f_k, f_{k+1}, f_{k+2}\}$, what choice of c supports cross-frequency coupling in the

network? To answer this, we choose $f_S = f_{k+2}$, $f_D = f_{k+1}$, and $f_T = f_k$ so that Equation (3c) becomes

$$f_{k+2} = f_{k+1} + f_k.$$

Substituting Equation (4) into this expression and solving for c, we find

$$c^2 - c - 1 = 0$$

with solution

$$c = \frac{1+\sqrt{5}}{2} = \phi,$$

the golden ratio. The same solution holds for all Equations (3) with appropriate selection of $\{f_S, f_D, f_T\}$ from $\{f_k, f_{k+1}, f_{k+2}\}$. We conclude that, for a system of damped coupled oscillators with oscillator and gain frequencies spaced by the multiplicative factor c, cross-frequency coupling between three neighboring rhythms requires $c = \phi$, the golden ratio. In other words, we propose that frequencies organized according to the golden ratio are particularly suited to support these cross-frequency interactions.

To illustrate this result, we consider a network of 8 damped, coupled oscillators each with a different natural frequency determined by the golden ratio ($f_k = \phi^k$, where $\phi = \frac{(1+\sqrt{5})}{2}$; Figure 2); we label these rhythms – scaled by factors of the golden ratio – as *golden rhythms*. Starting all nodes in a resting state, we perturb one oscillator ($f_D = \phi^6 \approx 17.9$ Hz) to produce a transient oscillation at that node. With only a constant gain ($\bar{g}_C = 50, \bar{g}_S = 0$), the impact of the perturbation on the other oscillators is small (Figure 2B); because $f_T \neq f_D$ for any oscillator pair, the network impact of the perturbation is small, despite the constant coupling.

Including the sinusoidal gain modulation ($\bar{g}_C = 50, \bar{g}_S = 50$) results in selective communication between the oscillators. For example, choosing $f_S = \phi^7 \approx 29.0$ Hz, we observe an evoked response at two oscillators (Figure 2C): $f_T = \phi^8 \approx 47.0$ Hz (consistent with Equation (3a)) and $f_T = \phi^5 \approx 11.1$ Hz (consistent with Equation (3c)). We note that the frequency of evoked responses matches the natural frequency of each oscillator. We also note that no solution exists for Equation (3b) because $f_T > 0$. Different choices of gain frequency f_S result in different pairs of cross-frequency coupling between the driver (f_D) and response oscillators (Figure 2D). Cross-frequency coupling occurs when Equations (3) are satisfied with $f_D \approx 17.9$ Hz. The coupling is selective; for example, choosing a gain modulation of $f_S = 11.1$ Hz results in cross-frequency coupling between the driver ($f_D = 17.9$ Hz) and faster (29 Hz) and slower (6.9 Hz) golden rhythms. In this case, sinusoidal gain frequencies f_S exist that support cross-frequency coupling and occur at factors of the golden ratio: i.e., $f_S = \phi^k$ (Figure 2D, circles). We note that evoked responses also occur when $f_S \neq \phi^k$ (Figure 2D, X's); in these cases, frequencies outside the original rhythm sequence $f_k = \phi^k$ must exist to support cross-frequency coupling. We conclude that if brain rhythmic

activity – both oscillator and gain frequencies – organizes according to the golden ratio, then cross-frequency coupling is possible between a subset of separate rhythmic communication channels.

We now consider the impact of noise on this cross-frequency communication. With sinusoidal gain modulation ($\bar{g}_c = 50$, $\bar{g}_s = 50$, and $f_S = \phi^7 \approx 29.0$ Hz) and including noise in the oscillator dynamics (see Methods), we show the results for two cases: with perturbation and without perturbation to one oscillator ($f_D \approx 17.9$ Hz, as above). Without perturbation (gray in Figure 2E), we find no evidence of an evoked response at any node, as expected; the amplitude remains small at all nodes, with a small gradual increase as the noise increases. With the perturbation (red in Figure 2E), we find an evoked response at the perturbed oscillator ($f_D \approx 17.9$ Hz) and two other oscillators: $f_T \approx 47.0$ Hz (consistent with Equation (3a)) and $f_T \approx 11.1$ Hz (consistent with Equation (3c)). As the noise increases, so does the variability in the evoked response. For the lower frequency $f_T \approx 11.1$ Hz oscillator, the evoked response remains evident as the noise increases; in Figure 2E, the perturbed (red) and unperturbed (gray) responses remain separate. For the higher frequency $f_T \approx 47.0$ Hz oscillator, the evoked response becomes more difficult to distinguish from the unperturbed case as the noise increases; in Figure 2E, the perturbed (red) and unperturbed (gray) responses begin to overlap with increasing noise. We note that the amplitude of evoked responses decreases with frequency. There-fore, the same amount of noise impacts the higher frequency ($f_T \approx 47.0$ Hz) oscillator more than the lower frequency ($f_T \approx 11.1$ Hz) oscillator, making an evoked response more difficult to distinguish from background noise in the higher frequency case. We also note that oscillators not satisfying Equation (3) (i.e., $f_T \approx \{6.9, 29.0, 76.0\}$ Hz when $f_D \approx 17.9$ Hz and $f_S \approx 29.0$ Hz) exhibit little evidence of an evoked response at any noise level.

To illustrate the utility of the golden ratio, we consider an alternative network of oscillators with frequencies organized by a factor of 2 (Figure 3A); such integer relationships have been proposed as important to neural communication [30, 55, 41]. As expected, with only constant gain ($\bar{g}_c = 50$) a perturbation to one node ($f_D = 16$ Hz) does not impact the rest of the network (Figure 3B). Including sinusoidal gain with frequency f_S can produce cross-frequency coupling. For example, choosing $f_S = 8$ Hz results in cross-frequency coupling between the $f_D = 16$ Hz and $f_T = 8$ Hz rhythms (Figure 3C). Similarly, choosing $f_S = 16$ Hz results in cross-frequency coupling between the $f_D = 16$ Hz and $f_T = 32$ Hz rhythms; however, this choice of f_S also results in strong cross-frequency coupling between $f_D = 16$ Hz and lower frequency rhythms ($f_T = 8, 4, 2, 1$ Hz; Figure 3D). Importantly, we note that cross-frequency coupling typically occurs at sinusoidal gain frequencies that differ from the set of oscillator frequencies at 2^k Hz (vertical lines in Figure 3D); a new set of rhythms (and rhythm generators) must exist to support cross-frequency coupling in this network.

To summarize, in a network of damped coupled oscillators (Equation 1), sinusoidal gain modulation supports cross-frequency coupling (Equation 3). If oscillator and gain frequencies organize according to a multiplicative factor (Equation 4), then cross-frequency coupling between neighboring frequencies requires a multiplicative factor of ϕ, the golden ratio (e.g., Figure 2D). While oscillators organized with a different multiplicative factor can still produce cross-frequency coupling, the frequencies of effective gain modulation

are not part of the original rhythmic sequence (e.g., Figure 3D), thus requiring the brain devote more resources to implementing a larger set of rhythms in support of cross-frequency interactions.

3.2 | plingRhythms organized by the golden ratio support ensembles of cross-frequency coupling

In the previous section, we considered a network of nodes oscillating at different natural frequencies. As an alternative example, we now consider a network with two ensembles of nodes oscillating at different frequencies. The two ensembles consist of nodes oscillating at frequencies ϕ^k or ϕ^{k+2}, where ϕ is the golden ratio. With only constant gain, a perturbation to any node impacts only nodes of the same ensemble (i.e., with the same frequency). Including sinusoidal gain modulation with (intermediate) frequency $f_S = \phi^{k+1}$, a perturbation to any node impacts nodes in both ensembles. We illustrate this in the 8-node network with 4 nodes in each ensemble oscillating at natural frequencies $\phi^4 \approx 6.85$ Hz or $\phi^6 \approx 17.9$ Hz (Figure 4A). With only constant gain ($\bar{g}_C = 50$, $\bar{g}_S = 0$), a perturbation to one $\phi^6 \approx 17.9$ Hz (driver) node impacts the amplitude of all other nodes in the same ensemble (Figure 4B). Including sinusoidal gain modulation ($\bar{g}_C = 50$, $\bar{g}_S = 50$) with frequency $\phi^5 \approx 11.1$ Hz, the same perturbation now impacts all nodes in both ensembles (Figure 4C). From Equation 3 we determine that two sinusoidal gain frequencies support cross-frequency coupling between the driver ($f_D = \phi^6 \approx 17.9$ Hz) and target ($f_T = \phi^4 \approx 6.85$ Hz) ensembles,

$$f_S = f_T - f_D = 6.85 - 17.9 < 0.00,$$

$$f_S = f_D - f_T = 17.9 - 6.85 = 11.1\text{Hz},$$

$$f_S = f_D + f_T = 17.9 + 6.85 = 24.6\text{Hz}.$$

However, of these two frequencies, only the former ($f_S = 11.1$ Hz) is also a golden rhythm (Figure 4D, box). In this case, cross-frequency coupling occurs when ensemble and gain rhythms organize in a "golden triplet" $(f_T, f_S, f_D) = (\phi^k, \phi^{k+1}, \phi^{k+2}) \approx (6.85, 11.1, 17.9)$ Hz, where $\phi^k + \phi^{k+1} = \phi^{k+2}$.

An alternative choice of irrational frequency ratio between the brain's rhythms is Euler's number (e) [40]. Repeating the simulation with two ensembles of frequency e^k or e^{k+2} results in cross-frequency coupling between ensembles only when $f_S = e^{k+2} \pm e^k$ (see Figure 5 for an example with $k = 2$). We therefore find similar results for the "Euler triplet" $(f_D, f_T, f_S) = (e^{k+2}, e^k, e^{k+2} \pm e^k)$ or specifically for $k = 2$, $(f_D, f_T, f_S) = (e^4, e^2, e^4 \pm e^2)$. However, this Euler triplet is not consistent with the ratio of e observed *in vivo*, where three neighboring frequency bands appear at multiplicative factors of e (e.g., $(f, ef, e^2 f)$) and the two slower rhythms do not sum to equal the faster rhythm (e.g., $f + ef \neq e^2 f$). Only for three neighboring frequency bands related by the golden ratio ($f, \phi f, \phi^2 f$) do the frequencies of the slower rhythms sum to the faster rhythm (i.e., $f + \phi f = \phi^2 f$).

3.3 | Golden rhythms establish a hierarchy of cross-frequency interactions

We now consider results derived for weakly coupled oscillators, which motivated the study of (strongly) coupled damped harmonic oscillators presented above. In [43, 44], Hoppensteadt and Izhikevich consider the general case of intrinsically oscillating neural populations with weak synaptic connections. When uncoupled, each neural population exhibits periodic activity (i.e., a stable limit cycle attractor) described by the phase of oscillation. We note that, in our study of coupled damped harmonic oscillators, we instead consider the amplitude of each oscillator. When Hoppensteadt and Izhikevich include weak synaptic connections between the neural populations, the phases of the neural populations interact only when a resonance relation exists between frequencies, i.e.,

$$\sum_i k_i f_i = 0,$$

where k_i is an integer and not all 0, and f_i is the frequency of neural population i. The resonance order is then defined as the summed magnitudes of the integers k_i,

$$\text{resonance order} = \sum_i \|k_i\| .$$

For the case of two neural populations, if

$$k_1 f_1 + k_2 f_2 = 0$$

for integers k_1 and k_2, then

$$\frac{f_2}{f_1} = -\frac{k_1}{k_2} = \text{ rational} .$$

In other words, if the frequency ratio f_2/f_1 of the two neural populations is rational (i.e., the ratio of two integers), then the neural populations may interact, with the strength of interaction decreasing as either k_1 or k_2 increases (i.e., stronger interactions correspond to smaller resonance orders)[1]. Alternatively, if this frequency ratio is irrational,

$$\frac{f_2}{f_1} = \text{ irrational},$$

then the two neural populations behave as if uncoupled.

Consistent with the results presented here, Hoppensteadt and Izhikevich show that golden triplets possess the lowest resonance order, and therefore the strongest cross-frequency coupling [43, 44, 45]. However, other resonances exist due to the recursive nature of rhythms organized by the golden ratio. To illustrate these relationships, we consider a set of golden rhythms $\{f^k\}$ – rhythms organized by the golden ratio so that,

[1] See Proposition 9.14 of [43]

$$f_{k-1} + f_k = f_{k+1}, \tag{6}$$

where k is an integer. Because

$$f_{k-1} + f_k - f_{k+1} = 0$$

the resonance order is 3; this golden triplet supports strong cross-rhythm communication. Replacing k with $k - 1$ in Equation 6, we find

$$f_{k-2} + f_{k-1} = f_k. \tag{7}$$

Then, replacing f_k in Equation 6 with the expression in Equation 7, we find

$$f_{k-1} + (f_{k-2} + f_{k-1}) = f_{k+1}$$

or

$$f_{k-2} + 2f_{k-1} - f_{k+1} = 0, \tag{8}$$

which has resonance order 4. Continuing this procedure to replace f_{k-2} in the equation above, we find

$$-f_{k-3} + 3f_{k-1} - f_{k+1} = 0, \tag{9}$$

which has resonance order 5. In this way, golden rhythms support specific patterns of preferred coupling between rhythmic triplets, with the strongest coupling (lowest resonance order) between golden triplets.

As a specific example, we fix $f_{k+1} = 40$ Hz and list in Table 1 the sequence of golden rhythms beginning with this generating frequency. We expect strong coupling between $(f_{k-1}, f_k, f_{k+1}) = (15.3, 25, 40)$ Hz, a golden triplet, which has resonance order 3. Using Equations 8, 9, and Table 1, we compute additional triplets with higher resonance orders: (9.4, 15.3, 40) Hz with resonance order 4, and (5.8, 15.3, 40) Hz with resonance order 5. Continuing this procedure organizes golden rhythms into triplets with different resonance orders (Figure 6). Triplets with low resonance order appear near the target frequency of $f_{k+1} = 40$ Hz (see gold, silver, and bronze circles in Figure 6), and resonance orders tend to increase for frequencies further from $f_{k+1} = 40$ Hz, with exceptions (e.g., $(f_{k-1}, f_k, f_{k+1}) = (2.2, 9.4, 40)$ Hz has resonance order 6). We conclude that - based on theory developed for weakly coupled oscillators - golden rhythms support both separate communication channels and a hierarchy of cross-frequency interactions between rhythmic triplets with varying coupling strengths. While here we consider three interacting rhythms, we note that the theory also applies to four (or more) interacting rhythms. The implications of these results for networks of (strongly) coupled (damped) oscillators remains unclear.

3.4 | Four experimental hypotheses

We propose that golden rhythms optimally support separate and integrated communication channels between oscillatory neural populations. We now describe four hypotheses deduced from this theory. First, if the organization of brain rhythms follows the golden ratio, then we expect a discrete sequence of three frequency bands subdivides the existing gamma frequency band, broadly defined from 30–100 Hz [37, 50], with peak frequencies separated by a factor of ϕ. For example, using the sequence of golden rhythms with generating frequency 40 Hz (Table 1), we identify multiple distinct rhythms (at 40 Hz, 65 Hz, 105 Hz) corresponding to this gamma band. Consistent with this hypothesis, multiple distinct rhythms have been identified within the gamma band (e.g., [56, 57, 58, 59, 60, 61, 62, 63, 64]). While different choices of generating frequency produce quantitatively different results, the qualitative result is the same: organized according to the golden ratio, multiple distinct rhythms exist within the gamma frequency range, each capable of supporting a separate communication channel.

Second, if rhythms organize according to the golden ratio, then evidence for this relationship should exist *in vivo*. To that end, we consider examples of two or more frequency bands reported in the literature (predominately in rodent hippocampus; Figure 7). These preliminary observations suggest that, in these cases, frequency bands separated by a factor of ϕ or ϕ^2 commonly occur.

Third, if rhythms organize according to the golden ratio, then we propose that rhythmic triplets support cross-frequency communication. Nearly all existing research in cross-frequency coupling focuses on interactions between two rhythms (e.g., theta-gamma [18, 28, 29]), and many measures exist to assess and interpret bivariate coupling between rhythms [29, 23, 65, 66]. Yet, brain rhythms coordinate beyond pairwise interactions; trivariate interactions between three brain rhythms include coordination of beta, low gamma, and high gamma activity by theta phase [31, 56, 57, 58, 62, 67]; coordination between ripples (140–200 Hz), sleep spindles (12–16 Hz), and slow oscillations (0.5–1.5 Hz) [20]; and coordination between (top-down) beta, (bottom-up) gamma, and theta rhythms [26]. To assess trivariate coupling, an obvious initial choice is the bicoherence, which assesses the phase relationship between three rhythms: f_1, f_2, and f_1+f_2 [68, 69, 70]. However, the bicoherence may be too restrictive (requiring a constant phase relationship between the three rhythms), and estimation of alternative interactions (e.g., between amplitudes and phases) will require application and development of alternative methods [71].

Fourth, why brain rhythms occur at the specific frequency bands observed, and not different bands, remains unknown. To address this, we combine the golden ratio scaling proposed here with a fundamental timescale for life on Earth: the time required for Earth to complete one rotation (i.e., the sidereal period) of 23 hr, 56 min. Beginning from this fundamental frequency (1/86160 Hz), we compute higher frequency bands by repeated multiplication of the golden ratio (Table 2). Doing so, we identify frequencies consistent with the canonical frequency bands (i.e., delta, theta, alpha, beta, low gamma, middle gamma, high gamma, ripples, fast ripples; see last column of Table 2). We note that broad frequency ranges define the canonical frequency bands, for example the gamma band from (30, 100) Hz. Therefore, model predictions that identify rhythms within a band is not surprising. We propose instead

that the relevant model prediction is the subdivision of the canonical frequency bands (e.g., the 10–30 Hz beta band into two sub-bands, the 30–100 Hz gamma band into three sub-bands), not the specific frequency values identified. We note that the lower frequencies may include "body oscillations", such as heart rate and breathing frequency [72], as proposed for a harmonic frequency relationship (factor of 2) in [41, 73]. We hypothesize that if intelligent life were to evolve on a planet like Earth, in a star system like our own, with neural physiology like our own, then rhythmic bands would exist with center frequencies that depend on the planet's circadian cycle. We acknowledge that this hypothesis, and the proposed association between neural rhythms and the sidereal period in Table 2, remain speculation, without robust supporting evidence.

4 | DISCUSSION

Why do brain rhythms organize into the small subset of discrete frequencies observed? Why does the alpha rhythm peak at 8–12 Hz and the (low) gamma rhythm peak at 35–55 Hz, across species [38]? Why does the brain not instead exhibit a continuum of rhythms, or a denser set of frequency bands, or different frequency bands? Here we provide a theoretical explanation for the organization of brain rhythms. Imposing a ratio of ϕ (the golden ratio) between the peaks of neighboring frequency bands, we constrain activity to a small subset of discrete brain rhythms, consistent with those observed *in vivo*. Organized in this way, brain rhythms optimally support the separation and integration of information in distinct rhythmic communication channels.

The framework proposed here combines insights developed in existing works. Mathematical analysis of weakly coupled oscillators established the importance of resonance order for effective communication between neural populations oscillating at different frequencies [43, 44, 45, 74]. Experimental observations and computational models have established the importance of brain rhythms [36, 39, 75], their interactions [18, 26], and their organization according to the golden ratio [42, 76, 77]. Here, we combine these previous results with simulations and analysis of a network of damped, coupled oscillators in support of the proposed theory.

The framework proposed here is consistent with existing theories for the role of brain rhythms. Like the communication-through-coherence (CTC) hypothesis [16, 26] and the frequency-division multiplexing hypothesis [12, 78], in the framework proposed here neural populations communicate dynamically along anatomical connections via coordinated rhythms. Organization by the golden ratio complements these existing theories in two ways. First, by proposing which rhythms participate – namely, rhythms spaced by factors of the golden ratio. Second, by proposing the importance of three rhythms to establish cross-frequency interactions and proposing a hierarchical organization to these interactions.

We considered a network of damped, coupled oscillators with sinusoidal gain modulation. In that network, cross-frequency coupling occurs when the gain frequency equals the sum or difference of the oscillator frequencies (Equation 3). This result holds without additional restrictions on the oscillator or gain frequencies. However, golden rhythms are unique in that oscillator and gain frequencies chosen from this set support cross-frequency

coupling; no rhythms beyond this set are required. Alternative irrational scaling factors (e.g., Euler's number e) establish different sets of oscillator frequencies (e.g.,… e^1, e^2, e^3,…) and separate communication channels, but require gain frequencies beyond this set to support cross-frequency coupling. In this alternative scenario, two distinct sets of rhythms exist: one reflecting local population activity, and another the cross-frequency coupling between populations. Rhythms organized by the golden ratio support a simpler framework: one set of frequencies (oscillator and gain) that reflect both local oscillations and their cross-frequency coupling. Golden rhythms are the smallest set of rhythms that support both separate communication channels and their cross-frequency interactions. Requiring fewer rhythms simplifies implementation, reducing the number of mechanisms required to produce these rhythms.

These results are consistent with existing proposals that the golden ratio organizes brain rhythms and minimizes cross-frequency interference [77, 79, 80]. We extend these proposals by showing how triplets of golden rhythms facilitate cross-frequency coupling. An integer ratio of 2 between frequency bands (with bandwidth determined by the golden ratio) provides an alternative organization to support cross-frequency coupling [41, 73]. In this scenario, cross-frequency interactions have been proposed to occur via a shift in frequency. For example, two regions - with an irrational frequency ratio - remain decoupled until the center frequencies shift to establish 1 : 2 phase coupling [81, 82]. We instead propose both regions maintain their original frequencies and couple when an appropriate third rhythm appears (e.g., a golden triplet). Our simulation results suggest more widespread coupling between populations oscillating at a 1 : 2 frequency ratio compared to a golden ratio (Figure 3D). Interpreted another way, integer ratios between frequency bands may facilitate a "coupling superhighway"; a target region shifts frequency to enter the coupling superhighway and receive strong inputs from all upstream regions oscillating at integer multiples (or factors) of the target frequency. Rhythms organized by a golden ratio require coordination with a third input to establish cross-frequency coupling. Investigating these proposals requires analysis of larger networks with multiple rhythms, and perhaps multiple organizing frequency ratios.

While we do not propose the specific mechanisms that support golden rhythms, proposals do exist. A biologically motivated sequence exists to create golden rhythms from the beta1 (15 Hz), beta2 (25 Hz), and gamma (40 Hz) bands. Through *in vitro* experiments and computational models, a process of period concatenation – in which the mechanisms producing the faster beta2 and gamma rhythms concatenate to create the slower beta1 rhythm – was proposed [77, 42, 76]. Alternatively, golden rhythms may emerge when two input rhythms undergo a nonlinear transformation [71, 83]. The framework proposed here suggests that the emergent rhythms – appearing at the sum and difference of the two rhythms – may support local coordination of the input rhythms.

The simplicity of the proposed framework (compared to the complexity of brain dynamics) results in at least four limitations. First, brain rhythms appear as broad spectral bands, not sharply defined spectral peaks. Therefore, the meaning of a precise frequency ratio, or the practical difference between an irrational frequency ratio (ϕ) and a rational frequency ratio (e.g., 1.6) is unclear. Second, rhythm frequencies may vary systematically and continuously

with respect to stimulus or behavioral parameters [84, 85]. Whether the brain maintains a constant frequency ratio between varying frequency rhythms, and what mechanisms could support this coordination, is unclear. Third, no evidence suggests the tuning of brain rhythms specifically to support separate communication channels. Instead, brain rhythms may occur at the frequencies observed due to the biological mechanisms available for coordination of neural activity (e.g., due to the decay time of inhibitory postsynaptic potentials that coordinate excitatory cell activity). Fourth, identification of rhythms in noisy brain signals remains a practical challenge, with numerous opportunities for confounds [64, 86, 87]. Therefore, the best approach to compare this theory with data remains unclear.

However, the simplicity of the golden framework is also an advantage. The framework consists of only one parameter (the golden ratio) compared to the many – typically poorly constrained – parameters of biologically detailed models of neural rhythms. In this way, the golden framework is broadly applicable and requires no specific biological mechanisms or rhythm frequencies; instead, only the relationship between frequencies is constrained.

No theoretical framework exists to explain the discrete set of brain rhythms observed in nature. Here, we propose a candidate framework, simply stated: brain rhythms are spaced according to the golden ratio. This simple statement implies brain rhythms establish communication channels optimal for separate and integrated information flow. While the specific purpose of brain rhythms remains unknown, perhaps the brain evolved to these rhythms in support of efficient multiplexing on a limited anatomical network.

Acknowledgements

The author would like to acknowledge Dr. Catherine Chu for writing assistance and tolerating many conversations about the golden ratio.

Funding information

NIH, NIBIB, Grant/Award Number: R01EB026938; NSF, Grant/Award Number: 1451384

A I: RELATIONSHIP BETWEEN A DAMPED HARMONIC OSCILLATOR AND AUTOREGRESSIVE MODEL OF ORDER TWO

Consider the damped harmonic oscillator driven by noise,

$$\ddot{x}_k + 2\beta\dot{x}_k + \omega_k^2 x_k = \xi(t),$$

where x is the position of the oscillator, β is the damping constant, ω_0 is the natural frequency, and $\xi(t)$ is a noise term evaluated at time t (e.g., see Equation (5.28) of [53]). Replacing each derivative with a discrete approximation we find,

$$\frac{x_t - 2x_{t-1} + x_{t-2}}{\Delta^2} + 2\beta\frac{x_t - x_{t-1}}{\Delta} + \omega_0^2 x_t = \xi_t,$$

where x_t is the oscillator position at discrete time t, and Δ is the time between t and $t+1$. Collecting terms at the same discrete time, we find,

$$\left(1 + 2\beta\Delta + \omega_0^2\Delta^2\right)x_t - 2(1 + \beta\Delta)x_{t-1} + x_{t-2} = \Delta^2\xi_t,$$

or

$$x_t = \alpha_1 x_{t-1} + \alpha_2 x_{t-2} + \epsilon_t, \tag{10}$$

where

$$\alpha_1 = \frac{2(1 + \beta\Delta)}{1 + 2\beta\Delta + \omega_0^2\Delta^2},$$

$$\alpha_2 = \frac{-1}{1 + 2\beta\Delta + \omega_0^2\Delta^2}$$

$$\epsilon_t = \Delta^2\xi_t.$$

Equation 10 defines an autoregressive model of order 2 (i.e., an AR(2)).

B I: RESONANCE RESPONSE FOR A DAMPED, DRIVEN OSCILLATOR WITH SINUSOIDAL GAIN

We begin with Equation 1,

$$\ddot{x}_k + 2\beta\dot{x}_k + \omega_k^2 x_k = (\bar{g}_C + \bar{g}_S\cos\omega_S t)\sum_{j \neq k} x_j, \tag{11}$$

and simplify by replacing each x_j with,

$$x_j \approx A_j\cos(\omega_j t);$$

i.e., we assume each input oscillator x_j oscillates with fixed amplitude (A_j) at its natural frequency (ω_j). Then Equation 11 becomes,

$$\ddot{x}_k + 2\beta\dot{x}_k + \omega_k^2 x_k = \bar{g}_C\sum_{j \neq k} A_j\cos(\omega_j t) + \bar{g}_S\cos(\omega_S t)\sum_{j \neq k} A_j\cos(\omega_j t). \tag{12}$$

Considering the first summation in Equation 12 for the j^{th} oscillator,

$$\ddot{x}_k + 2\beta\dot{x}_k + \omega_k^2 x_k = \bar{g}_C A_j\cos(\omega_j t).$$

and applying the standard approach to solving a damped oscillator with sinusoidal driving force (e.g., see Chapter 5 of [53]), we determine the amplitude A_k of the driven oscillator,

$$A_k^2 = \frac{\bar{g}_C^2 A_j^2}{\left(\omega_k^2 - \omega_j^2\right)^2 + 4\beta^2\omega_j^2}. \tag{13}$$

The amplitude of the driven oscillator is largest when $\omega_j = \omega_k$, i.e., when the frequency of the driving oscillator ω_j equals the natural frequency of the driven oscillator ω_k.

We now consider the second summation in Equation 12 for the j^{th} oscillator,

$$\ddot{x}_k + 2\beta\dot{x}_k + \omega_k^2 x_k = \bar{g}_S A_j \cos(\omega_j t)\cos(\omega_S t)$$
$$= \frac{\bar{g}_S A_j}{2}\cos((\omega_j - \omega_S)t) + \cos((\omega_j + \omega_S)t).$$

Any solution to this equation must also satisfy,

$$\ddot{x}_k + 2\beta\dot{x}_k + \omega_k^2 x_k = \frac{\bar{g}_S A_j}{2}\sin((\omega_j - \omega_S)t) + \sin((\omega_j + \omega_S)t).$$

We define $z_k = x_k + iy_k$ and combine the two previous equations to find,

$$\ddot{z}_k + 2\beta\dot{z}_k + \omega_k^2 z_k = \frac{\bar{g}_S A_j}{2}e^{i(\omega_j - \omega_S)t} + \frac{\bar{g}_S A_j}{2}e^{i(\omega_j + \omega_S)t}.$$

We now apply the standard approach to solving a damped oscillator with sinusoidal driving force (e.g., see Chapter 5 of [53]) to determine the amplitude B_k of the driven oscillator,

$$B_k^2 = \frac{\bar{g}_C^2 A_j^2/4}{\left(\omega_k^2 - (\omega_j \pm \omega_S)^2\right)^2 + 4\beta^2(\omega_j \pm \omega_S)^2}.$$

The amplitude B_k is largest when,

$$\omega_k^2 = (\omega_j \pm \omega_S)^2,$$

which is satisfied when,

$$\begin{aligned} \omega_j + \omega_S = \omega_k \quad &\rightarrow \quad \omega_S = \omega_k - \omega_j, \\ \omega_j - \omega_S = \omega_k \quad &\rightarrow \quad \omega_S = \omega_j - \omega_k. \end{aligned} \tag{14}$$

Considering the equivalent expression,

$$\omega_k^2 = (-1)^2(\omega_j \pm \omega_S)^2 = (-\omega_j \mp \omega_S)^2,$$

we find an additional solution,

$$-\omega_j + \omega_S = \omega_k \quad \rightarrow \quad \omega_S = \omega_k + \omega_j \,. \tag{15}$$

We conclude that the amplitude of the driven oscillator B_k is largest when the frequency of the sinusoidal gain modulation ω_S equals the difference (Equation 14) or sum (Equation 15) of the natural frequencies of the driven ω_k and driving ω_j oscillators.

References

[1]. Hipp JF, Engel AK, Siegel M. Oscillatory Synchronization in Large-Scale Cortical Networks Predicts Perception. Neuron 2011 Jan;69(2):387–396. https://www.sciencedirect.com/science/article/pii/S0896627310010755. [PubMed: 21262474]

[2]. Vezoli J, Vinck M, Bosman CA, Bastos AM, Lewis CM, Kennedy H, et al. Brain rhythms define distinct interaction networks with differential dependence on anatomy. Neuron 2021 Oct;https://www.sciencedirect.com/science/article/pii/S089662732100725X.

[3]. Engel AK, Fries P, Singer W. Dynamic predictions: Oscillations and synchrony in top–down processing. Nature Reviews Neuroscience 2001 Oct;2(10):704–716. https://www.nature.com/articles/35094565, bandiera_abtest: a Cg_type: Nature Research Journals Number: 10 Primary_atype: Reviews Publisher: Nature Publishing Group. [PubMed: 11584308]

[4]. Salinas E, Sejnowski TJ. Correlated neuronal activity and the flow of neural information. Nature Reviews Neuroscience 2001 Aug;2(8):539–550. https://www.nature.com/articles/35086012, bandiera_abtest: a Cg_type: Nature Research Journals Number: 8 Primary_atype: Reviews Publisher: Nature Publishing Group. [PubMed: 11483997]

[5]. Fox MD, Raichle ME. Spontaneous fluctuations in brain activity observed with functional magnetic resonance imaging. Nature Reviews Neuroscience 2007 Sep;8(9):700–711. http://www.nature.com/nrn/journal/v8/n9/full/nrn2201.html. [PubMed: 17704812]

[6]. Brookes MJ, Woolrich M, Luckhoo H, Price D, Hale JR, Stephenson MC, et al. Investigating the electrophysiological basis of resting state networks using magnetoencephalography. Proceedings of the National Academy of Sciences 2011 Oct;108(40):16783–16788. http://www.pnas.org/cgi/doi/10.1073/pnas.1112685108.

[7]. de Pasquale F, Della Penna S, Snyder AZ, Marzetti L, Pizzella V, Romani GL, et al. A Cortical Core for Dynamic Integration of Functional Networks in the Resting Human Brain. Neuron 2012 May;74(4):753–764. https://www.sciencedirect.com/science/article/pii/S089662731200342X. [PubMed: 22632732]

[8]. Kopell NJ, Gritton HJ, Whittington MA, Kramer MA. Beyond the connectome: the dynome. Neuron 2014 Sep;83(6):1319–1328. [PubMed: 25233314]

[9]. Quiroga RQ. Closing the gap between mind and brain with the dynamic connectome. Proceedings of the National Academy of Sciences 2020 May;117(18):9677–9678. http://www.pnas.org/content/117/18/9677, publisher: National Academy of Sciences Section: Commentary..

[10]. Tononi G An information integration theory of consciousness. BMC Neuroscience 2004;5(1):42. http://bmcneurosci.biomedcentral.com/articles/10.1186/1471-2202-5-42. [PubMed: 15522121]

[11]. Kohn A, Jasper AI, Semedo JD, Gokcen E, Machens CK, Yu BM. Principles of Corticocortical Communication: Proposed Schemes and Design Considerations. Trends in Neurosciences 2020 Sep;43(9):725–737. https://linkinghub.elsevier.com/retrieve/pii/S016622362030165X. [PubMed: 32771224]

[12]. Akam T, Kullmann DM. Oscillatory multiplexing of population codes for selective communication in the mammalian brain. Nature Reviews Neuroscience 2014 Jan; http://www.nature.com/nrn/journal/v15/n2/full/nrn3668.html.

[13]. Becker R, Hervais-Adelman A. Resolving the Connectome, Spectrally-Specific Functional Connectivity Networks and Their Distinct Contributions to Behavior. eNeuro 2020 Sep;7(5). https://www.eneuro.org/content/7/5/ENEURO.0101-20.2020, publisher: Society for Neuroscience Section: Research Article: New Research.

[14]. Hahn G, Ponce-Alvarez A, Deco G, Aertsen A, Kumar A.Portraits of communication in neuronal networks. Nature Reviews Neuroscience 2019 Feb;20(2):117–127. http://www.nature.com/articles/s41583-018-0094-0, bandiera_abtest: a Cg_type: Nature Research Journals Number: 2 Primary_atype: Reviews Publisher: Nature Publishing Group Subject_term: Network models;Neural circuits Subject_term_id: network-models;neural-circuit. [PubMed: 30552403]

[15]. Palmigiano A, Geisel T, Wolf F, Battaglia D. Flexible information routing by transient synchrony. Nature Neuroscience 2017 Jul;20(7):1014–1022. http://www.nature.com/articles/nn.4569, bandiera_abtest: a Cg_type: Nature Research Journals Number: 7 Primary_atype: Research Publisher: Nature Publishing Group Subject_term: Attention;Network models Subject_term_id: attention;network-models. [PubMed: 28530664]

[16]. Fries P A mechanism for cognitive dynamics: neuronal communication through neuronal coherence. Trends in Cognitive Sciences 2005 Oct;9(10):474–480. http://www.sciencedirect.com/science/article/pii/S1364661305002421. [PubMed: 16150631]

[17]. González J, Cavelli M, Mondino A, Rubido N, BL Tort A, Torterolo P. Communication Through Coherence by Means of Cross-frequency Coupling. Neuroscience 2020 Nov;449:157–164. https://www.sciencedirect.com/science/article/pii/S0306452220305935. [PubMed: 32926953]

[18]. Canolty RT, Knight RT.The functional role of cross-frequency coupling. Trends in Cognitive Sciences 2010 Nov;14(11):506–515. http://www.sciencedirect.com/science?_ob=ArticleURL&_udi=B6VH9-51620R1-1&_user=489277&_coverDate=11%2F30%2F2010&_rdoc=1&_fmt=high&_orig=search&_origin=search&_sort=d&_docanchor=&view=c&_acct=C000022679&_version=1&_urlVersion=0&_userid=489277&md5=c81841417ceb844440208c1c8b2fb189&searchtype=a. [PubMed: 20932795]

[19]. Bonnefond M, Kastner S, Jensen O. Communication between Brain Areas Based on Nested Oscillations. eNeuro 2017 Mar;4(2). https://www.eneuro.org/content/4/2/ENEURO.0153-16.2017, publisher: Society for Neuroscience Section: Theory/New Concepts.

[20]. Buzsáki G, Watson BO. Brain rhythms and neural syntax: implications for efficient coding of cognitive content and neuropsychiatric disease. Dialogues in Clinical Neuroscience 2012 Dec;14(4):345–367. https://www.ncbi.nlm.nih.gov/pmc/articles/PMC3553572/. [PubMed: 23393413]

[21]. Palva S, Palva JM. Discovering oscillatory interaction networks with M/EEG: challenges and breakthroughs. Trends in Cognitive Sciences 2012 Apr;16(4):219–230. https://www.sciencedirect.com/science/article/pii/S1364661312000472. [PubMed: 22440830]

[22]. Siegel M, Donner TH, Engel AK. Spectral fingerprints of large-scale neuronal interactions. Nature Reviews Neuroscience 2012 Feb;13(2):121–134. http://www.nature.com/nrn/journal/v13/n2/full/nrn3137.html. [PubMed: 22233726]

[23]. Siebenhühner F, Wang SH, Arnulfo G, Lampinen A, Nobili L, Palva JM, et al. Genuine cross-frequency coupling networks in human resting-state electrophysiological recordings. PLOS Biology 2020 May;18(5):e3000685. https://journals.plos.org/plosbiology/article?id=10.1371/journal.pbio.3000685, publisher: Public Library of Science. [PubMed: 32374723]

[24]. Williams N, Wang SH, Arnulfo G, Nobili L, Palva S, Palva JM. Modules in connectomes of phase-synchronization comprise anatomically contiguous, functionally related regions; 2021.

[25]. Bastos AM, Vezoli J, Fries P. Communication through coherence with inter-areal delays. Current Opinion in Neurobiology 2015 Apr;31:173–180. http://www.sciencedirect.com/science/article/pii/S0959438814002165. [PubMed: 25460074]

[26]. Fries P Rhythms for Cognition: Communication through Coherence. NEURON 2015 Oct;88(1):220–235. 10.1016/j.neuron.2015.09.034. [PubMed: 26447583]

[27]. Schroeder CE, Lakatos P. Low-frequency neuronal oscillations as instruments of sensory selection. Trends in Neurosciences 2009 Jan;32(1):9–18. https://www.sciencedirect.com/science/article/pii/S0166223608002506. [PubMed: 19012975]

[28]. Lisman JE, Jensen O. The Theta-Gamma Neural Code. NEURON 2013 Mar;77(6):1002–1016. http://linkinghub.elsevier.com/retrieve/pii/S0896627313002316. [PubMed: 23522038]

[29]. Hyafil A, Giraud AL, Fontolan L, Gutkin B. Neural Cross-Frequency Coupling: Connecting Architectures, Mechanisms, and Functions. Trends in Neurosciences 2015 Nov;38(11):725–740. http://eutils.ncbi.nlm.nih.gov/entrez/eutils/elink.fcgi?dbfrom=pubmed&id=26549886&retmode=ref&cmd=prlinks. [PubMed: 26549886]

[30]. Palva JM, Palva S, Kaila K. Phase Synchrony among Neuronal Oscillations in the Human Cortex. Journal of Neuroscience 2005 Apr;25(15):3962–3972. https://www.jneurosci.org/content/25/15/3962, publisher: Society for Neuroscience Section: Behavioral/Systems/Cognitive. [PubMed: 15829648]

[31]. Belluscio MA, Mizuseki K, Schmidt R, Kempter R, Buzsaki G. Cross-Frequency Phase-Phase Coupling between Theta and Gamma Oscillations in the Hippocampus. Journal of Neuroscience 2012 Jan;32(2):423–435. http://www.jneurosci.org/cgi/doi/10.1523/JNEUROSCI.4122-11.2012. [PubMed: 22238079]

[32]. Tass P, Rosenblum MG, Weule J, Kurths J, Pikovsky A, Volkmann J, et al. Detection of n : m Phase Locking from Noisy Data: Application to Magnetoencephalography. Physical Review Letters 1998 Oct;81(15):3291–3294. https://link.aps.org/doi/10.1103/PhysRevLett.81.3291.

[33]. Lundqvist M, Rose J, Herman P, Brincat SL, Buschman TJ, Miller EK. Gamma and Beta Bursts Underlie Working Memory. Neuron 2016 Apr;90(1):152–164. https://www.sciencedirect.com/science/article/pii/S0896627316001458. [PubMed: 26996084]

[34]. Sherman MA, Lee S, Law R, Haegens S, Thorn CA, Hämäläinen MS, et al. Neural mechanisms of transient neocortical beta rhythms: Converging evidence from humans, computational modeling, monkeys, and mice. Proceedings of the National Academy of Sciences 2016 Aug;113(33):E4885–E4894. http://www.pnas.org/content/113/33/E4885, publisher: National Academy of Sciences Section: PNAS Plus.

[35]. van Ede F, Quinn AJ, Woolrich MW, Nobre AC. Neural Oscillations: Sustained Rhythms or Transient Burst-Events? Trends in Neurosciences 2018 Jul;41(7):415–417. https://linkinghub.elsevier.com/retrieve/pii/S0166223618301036. [PubMed: 29739627]

[36]. Buzsaki G Rhythms of the Brain. Oxford University Press; 2011.

[37]. Buzsaki G, Draguhn A. Neuronal Oscillations in Cortical Networks. Science 2004 Jun;304(5679):1926–1929. https://www.sciencemag.org/lookup/doi/10.1126/science.1099745. [PubMed: 15218136]

[38]. Buzsáki G, Logothetis N, Singer W. Scaling Brain Size, Keeping Timing: Evolutionary Preservation of Brain Rhythms. Neuron 2013 Oct;80(3):751–764. http://www.sciencedirect.com/science/article/pii/S0896627313009045. [PubMed: 24183025]

[39]. Whittington M, Traub R, Kopell N, Ermentrout B, Buhl E. Inhibition-based rhythms: experimental and mathematical observations on network dynamics. Int J Psychophysiol 2000 Dec;38(3):315–336. [PubMed: 11102670]

[40]. Penttonen M, Buzsáki G. Natural logarithmic relationship between brain oscillators. Thalamus & Related Systems 2003 Apr;2(2):145–152. http://www.sciencedirect.com/science/article/pii/S1472928803000074.

[41]. Klimesch W An algorithm for the EEG frequency architecture of consciousness and brain body coupling. Frontiers in Human Neuroscience 2013;7. https://www.frontiersin.org/articles/10.3389/fnhum.2013.00766/full, publisher: Frontiers.

[42]. Roopun AK, Kramer MA, Carracedo LM, Kaiser M, Davies CH, Traub RD, et al. Temporal Interactions between Cortical Rhythms. Frontiers in neuroscience 2008 Dec;2(2):145–154. http://www.frontiersin.org/neuroscience/paper/10.3389/neuro.01/034.2008/, publisher: Frontiers. [PubMed: 19225587]

[43]. Izhikevich EM, Hoppensteadt FC. Weakly Connected Neural Networks. 1st ed. Springer; 1997.

[44]. Hoppensteadt FC, Izhikevich EM. Thalamo-cortical interactions modeled by weakly connected oscillators: could the brain use FM radio principles? Biosystems 1998 Nov;48(1–3):85–94. https://linkinghub.elsevier.com/retrieve/pii/S0303264798000537. [PubMed: 9886635]

[45]. Izhikevich EM. Weakly Connected Quasi-periodic Oscillators, FM Interactions, and Multiplexing in the Brain. SIAM Journal on Applied Mathematics 1999 Jan;59(6):2193–2223. https://epubs.siam.org/doi/abs/10.1137/S0036139997330623, publisher: Society for Industrial and Applied Mathematics.

[46]. Michalareas G, Vezoli J, van Pelt S, Schoffelen JM, Kennedy H, Fries P. Alpha-Beta and Gamma Rhythms Subserve Feedback and Feedforward Influences among Human Visual Cortical Areas. Neuron 2016 Jan;89(2):384–397. https://linkinghub.elsevier.com/retrieve/pii/S0896627315011204. [PubMed: 26777277]

[47]. Fontolan L, Morillon B, Liegeois-Chauvel C, Giraud AL. The contribution of frequency-specific activity to hierarchical information processing in the human auditory cortex. Nature communications 2014 Sep;5. https://www.nature.com/articles/ncomms5694.

[48]. Bastos AM, Lundqvist M, Waite AS, Kopell N, Miller EK. Layer and rhythm specificity for predictive routing. Proceedings of the National Academy of Sciences 2020 Dec;117(49):31459–31469. http://www.pnas.org/content/117/49/31459, publisher: National Academy of Sciences Section: Biological Sciences.

[49]. Moorman CM, Goff JE. Golden ratio in a coupled-oscillator problem. European Journal of Physics 2007 Sep;28(5):897–902. https://iopscience.iop.org/article/10.1088/0143-0807/28/5/013.

[50]. Fries P, Nikolić D, Singer W. The gamma cycle. Trends in Neurosciences 2007 Jul;30(7):309–316. https://www.sciencedirect.com/science/article/pii/S0166223607001245. [PubMed: 17555828]

[51]. Izhikevich EM. Synchronization of Elliptic Bursters. SIAM Review 2001 Jan;43(2):315–344. http://epubs.siam.org/doi/10.1137/S0036144500382064.

[52]. Spyropoulos G, Dowdall JR, Schölvinck ML, Bosman CA, Lima B, Peter A, et al. Spontaneous variability in gamma dynamics described by a linear harmonic oscillator driven by noise. bioRxiv 2020 May;p. 793729. https://www.biorxiv.org/content/10.1101/793729v2, publisher: Cold Spring Harbor Laboratory Section: New Results.

[53]. Taylor J Classical Mechanics. University Science Books; 2005.

[54]. Akam T, Kullmann DM. Oscillations and Filtering Networks Support Flexible Routing of Information. Neuron 2010 Jul;67(2):308–320. https://www.cell.com/neuron/abstract/S0896-6273(10)00477-0. [PubMed: 20670837]

[55]. Marín García AO, Müller MF, Schindler K, Rummel C. Genuine cross-correlations: which surrogate based measure reproduces analytical results best? Neural networks : the official journal of the International Neural Network Society 2013 Oct;46:154–164. http://www.sciencedirect.com/science/article/pii/S0893608013001482. [PubMed: 23751366]

[56]. Lopes-dos Santos V, van de Ven GM, Morley A, Trouche S, Campo-Urriza N, Dupret D. Parsing Hippocampal Theta Oscillations by Nested Spectral Components during Spatial Exploration and Memory-Guided Behavior. Neuron 2018 Nov;100(4):940–952. https://linkinghub.elsevier.com/retrieve/pii/S089662731830833X. [PubMed: 30344040]

[57]. Zhang L, Lee J, Rozell C, Singer AC. Sub-second dynamics of theta-gamma coupling in hippocampal CA1. eLife 2019 Jul;8:e44320. 10.7554/eLife.44320, publisher: eLife Sciences Publications, Ltd. [PubMed: 31355744]

[58]. Fernández-Ruiz A, Oliva A, Nagy GA, Maurer AP, Berényi A, Buzsáki G. Entorhinal-CA3 Dual-Input Control of Spike Timing in the Hippocampus by Theta-Gamma Coupling. Neuron 2017 Mar;93(5):1213–1226.e5. http://www.sciencedirect.com/science/article/pii/S0896627317301010. [PubMed: 28279355]

[59]. Edwards E, Soltani M, Deouell LY, Berger MS, Knight RT. High Gamma Activity in Response to Deviant Auditory Stimuli Recorded Directly From Human Cortex. Journal of Neurophysiology 2005 Dec;94(6):4269–4280. https://journals.physiology.org/doi/full/10.1152/jn.00324.2005, publisher: American Physiological Society. [PubMed: 16093343]

[60]. Crone NE, Miglioretti DL, Gordon B, Lesser RP. Functional mapping of human sensorimotor cortex with electrocortico-graphic spectral analysis. II. Event-related synchronization in the gamma band. Brain 1998 Dec;121(12):2301–2315. 10.1093/brain/121.12.2301. [PubMed: 9874481]

[61]. Vidal JR, Chaumon M, O'Regan JK, Tallon-Baudry C. Visual Grouping and the Focusing of Attention Induce Gamma-band Oscillations at Different Frequencies in Human Magnetoencephalogram Signals. Journal of Cognitive Neuroscience 2006 Nov;18(11):1850–1862. 10.1162/jocn.2006.18.11.1850. [PubMed: 17069476]

[62]. Colgin LL, Denninger T, Fyhn M, Hafting T, Bonnevie T, Jensen O, et al. Frequency of gamma oscillations routes flow of information in the hippocampus. Nature 2009 Nov;462(7271):353–357. https://www.nature.com/articles/nature08573, bandiera_abtest: a Cg_type: Nature Research Journals Number: 7271 Primary_atype: Research Publisher: Nature Publishing Group. [PubMed: 19924214]

[63]. Colgin LL. Do slow and fast gamma rhythms correspond to distinct functional states in the hippocampal network? Brain research 2015 Sep;1621:309–315. https://www.ncbi.nlm.nih.gov/pmc/articles/PMC4499490/. [PubMed: 25591484]

[64]. Zhou Y, Sheremet A, Qin Y, Kennedy JP, DiCola NM, Burke SN, et al. Methodological Considerations on the Use of Different Spectral Decomposition Algorithms to Study Hippocampal Rhythms. eNeuro 2019 Jul;https://www.eneuro.org/content/early/2019/07/19/ENEURO.0142-19.2019, publisher: Society for Neuroscience Section: Theory/New Concepts.

[65]. Tort ABL, Komorowski R, Eichenbaum H, Kopell N. Measuring phase-amplitude coupling between neuronal oscillations of different frequencies. Journal of Neurophysiology 2010 Aug;104(2):1195–1210. http://jn.physiology.org/content/104/2/1195.long. [PubMed: 20463205]

[66]. Aru J, Aru J, Priesemann V, Wibral M, Lana L, Pipa G, et al. Untangling cross-frequency coupling in neuroscience. Current Opinion in Neurobiology 2015 Apr;31:51–61. https://linkinghub.elsevier.com/retrieve/pii/S0959438814001640. [PubMed: 25212583]

[67]. Jiang H, Bahramisharif A, Gerven MAJv, Jensen O. Distinct directional couplings between slow and fast gamma power to the phase of theta oscillations in the rat hippocampus. European Journal of Neuroscience 2020;51(10):2070–2081. http://onlinelibrary.wiley.com/doi/abs/10.1111/ejn.14644, _eprint: https://onlinelibrary.wiley.com/doi/pdf/10.1111/ejn.14644. [PubMed: 31834955]

[68]. Barnett TP, Johnson LC, Naitoh P, Hicks N, Nute C. Bispectrum Analysis of Electroencephalogram Signals during Waking and Sleeping. Science 1971 Apr;172(3981):401–402. http://www.science.org/doi/10.1126/science.172.3981.401, publisher: American Association for the Advancement of Science. [PubMed: 5550492]

[69]. Kramer MA, Tort ABL, Kopell NJ. Sharp edge artifacts and spurious coupling in EEG frequency comodulation measures. Journal of Neuroscience Methods 2008 May;170(2):352–357. http://www.sciencedirect.com/science?_ob=ArticleURL&_udi=B6T04-4RRFN6B-2&_user=489277&_rdoc=1&_fmt=&_orig=search&_sort=d&_docanchor=&view=c&_acct=C000022679&_version=1&_urlVersion=0&_userid=489277&md5=b3573556b26c14876c9fe80c26c670c0. [PubMed: 18328571]

[70]. Shahbazi Avarvand F, Bartz S, Andreou C, Samek W, Leicht G, Mulert C, et al. Localizing bicoherence from EEG and MEG. NeuroImage 2018 Jul;174:352–363. https://linkinghub.elsevier.com/retrieve/pii/S1053811918300442. [PubMed: 29421325]

[71]. Haufler D, Paré D. Detection of Multiway Gamma Coordination Reveals How Frequency Mixing Shapes Neural Dynamics. Neuron 2019 Feb;101(4):603–614.e6. https://www.sciencedirect.com/science/article/pii/S0896627318311486. [PubMed: 30679018]

[72]. Tort ABL, Brankačk J, Draguhn A. Respiration-Entrained Brain Rhythms Are Global but Often Overlooked. Trends in Neurosciences 2018 Apr;41(4):186–197. https://www.sciencedirect.com/science/article/pii/S0166223618300316. [PubMed: 29429805]

[73]. Klimesch W The frequency architecture of brain and brain body oscillations: an analysis. European Journal of Neuroscience 2018;48(7):2431–2453. https://www.onlinelibrary.wiley.com/doi/abs/10.1111/ejn.14192, _eprint: https://onlinelibrary.wiley.com/doi/pdf/10.1111/ejn.14192. [PubMed: 30281858]

[74]. Brain Nunez P., Mind, and the Structure of Reality. 1st ed. Oxford University Press; 2010.

[75]. Wang XJ. Neurophysiological and computational principles of cortical rhythms in cognition. Physiological Reviews 2010 Jul;90(3):1195–1268. http://physrev.physiology.org/content/90/3/1195.long. [PubMed: 20664082]

[76]. Kramer MA, Roopun AK, Carracedo LM, Traub RD, Whittington MA, Kopell NJ. Rhythm Generation through Period Concatenation in Rat Somatosensory Cortex. PLOS Computational Biology 2008 Sep;4(9):e1000169. https://journals.plos.org/ploscompbiol/article?id=10.1371/journal.pcbi.1000169, publisher: Public Library of Science. [PubMed: 18773075]

[77]. Roopun AK, Kramer MA, Carracedo LM, Kaiser M, Davies CH, Traub RD, et al. Period concatenation underlies interactions between gamma and beta rhythms in neocortex. Frontiers in Cellular Neuroscience 2008;2. https://www.frontiersin.org/articles/10.3389/neuro.03.001.2008/full, publisher: Frontiers.

[78]. Akam TE, Kullmann DM. Efficient “Communication through Coherence” Requires Oscillations Structured to Minimize Interference between Signals. PLOS Computational

Biology 2012 Nov;8(11):e1002760. https://journals.plos.org/ploscompbiol/article?id=10.1371/journal.pcbi.1002760, publisher: Public Library of Science. [PubMed: 23144603]

[79]. Weiss H, Weiss V. The golden mean as clock cycle of brain waves. Chaos, Solitons & Fractals 2003 Nov;18(4):643–652. http://www.sciencedirect.com/science/article/pii/S0960077903000262.

[80]. Pletzer B, Kerschbaum H, Klimesch W. When frequencies never synchronize: The golden mean and the resting EEG. Brain Research 2010 Jun;1335:91–102. http://www.sciencedirect.com/science/article/pii/S0006899310007092. [PubMed: 20350536]

[81]. Rodriguez-Larios J, Wong KF, Lim J, Alaerts K. Mindfulness Training is Associated with Changes in Alpha-Theta Cross-Frequency Dynamics During Meditation. Mindfulness 2020 Dec;11(12):2695–2704. 10.1007/s12671-020-01487-3.

[82]. Rodriguez-Larios J, Faber P, Achermann P, Tei S, Alaerts K. From thoughtless awareness to effortful cognition: alpha - theta cross-frequency dynamics in experienced meditators during meditation, rest and arithmetic. Scientific Reports 2020 Mar;10(1):5419. https://www.nature.com/articles/s41598-020-62392-2, bandiera_abtest: a Cc_license_type: cc_by Cg_type: Nature Research Journals Number: 1 Primary_atype: Research Publisher: Nature Publishing Group Subject_term: Cognitive control;Cognitive neuroscience Subject_term_id: cognitive-control;cognitive-neuroscience. [PubMed: 32214173]

[83]. Ahrens KF, Levine H, Suhl H, Kleinfeld D. Spectral mixing of rhythmic neuronal signals in sensory cortex. Proceedings of the National Academy of Sciences 2002 Nov;99(23):15176–15181. https://www.pnas.org/content/99/23/15176, publisher: National Academy of Sciences Section: Biological Sciences.

[84]. Ray S, Maunsell JHR. Differences in Gamma Frequencies across Visual Cortex Restrict Their Possible Use in Computation. Neuron 2010 Sep;67(5):885–896. https://www.sciencedirect.com/science/article/pii/S0896627310006148. [PubMed: 20826318]

[85]. Kropff E, Carmichael JE, Moser EI, Moser MB. Frequency of theta rhythm is controlled by acceleration, but not speed, in running rats. Neuron 2021 Mar;109(6):1029–1039.e8. https://linkinghub.elsevier.com/retrieve/pii/S0896627321000398. [PubMed: 33567253]

[86]. Cole SR, Voytek B. Brain Oscillations and the Importance of Waveform Shape. Trends in Cognitive Sciences 2017 Jan;21(2):137–149. http://linkinghub.elsevier.com/retrieve/pii/S1364661316302182. [PubMed: 28063662]

[87]. Donoghue T, Schaworonkow N, Voytek B. Methodological considerations for studying neural oscillations. European Journal of Neuroscience 2021;http://onlinelibrary.wiley.com/doi/abs/10.1111/ejn.15361, _eprint: https://onlinelibrary.wiley.com/doi/pdf/10.1111/ejn.15361.

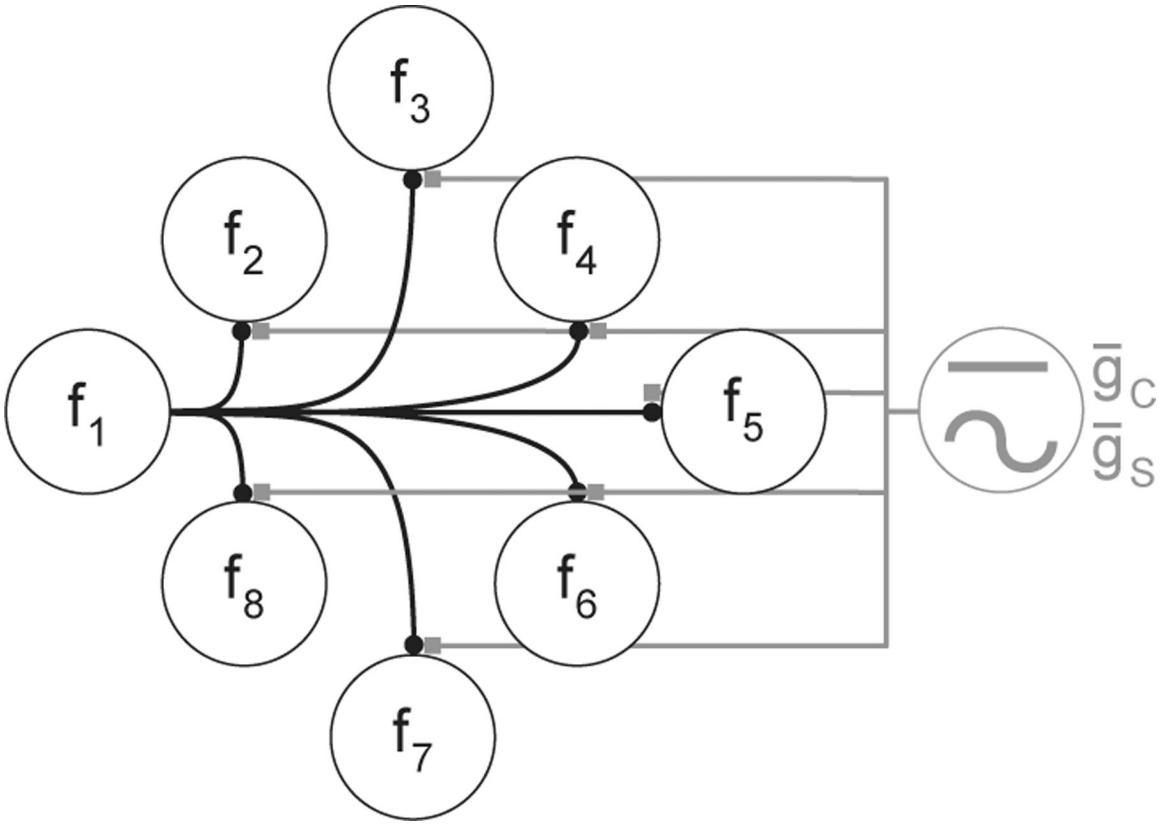

FIGURE 1. Illustration of the coupled oscillator network.

Oscillators with frequency f_k receive input from all other oscillators. Input from one oscillator (frequency f_1) to all other oscillators (f_2, f_3,…, f_8) is shown (black curves); similar connectivities exist from all other oscillators (not shown). Constant ($\bar{g}_c$) and sinusoidal ($\bar{g}_s$) gain modulates each input (gray lines).

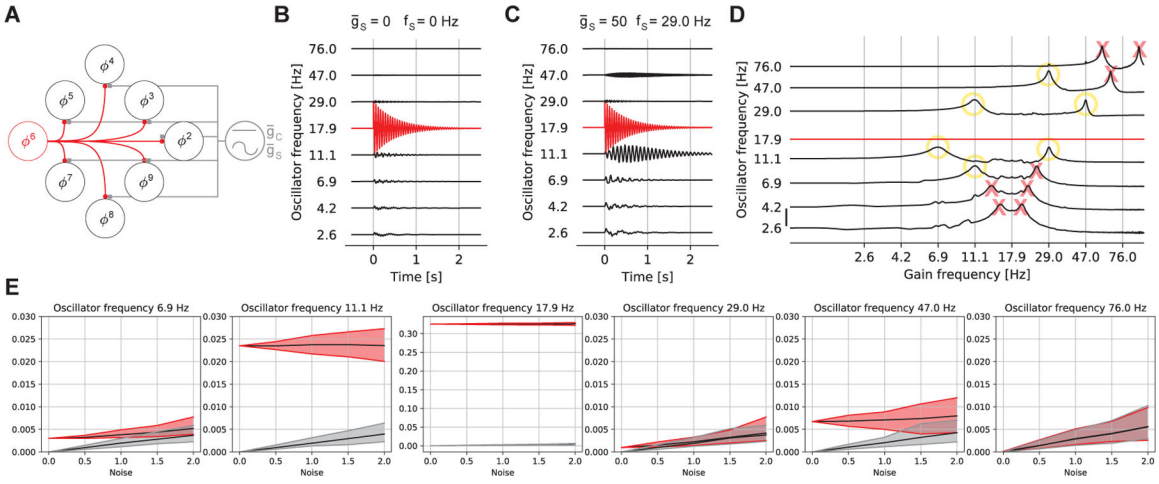

FIGURE 2. Rhythms organized by the golden ratio support selective cross-frequency coupling.
(A) We perturb one oscillator (natural frequency 17.9 Hz, red), with connectivity to all other oscillators; ϕ is the golden ratio. **(B)** With only constant gain modulation, the perturbation (t = 0, red) has little impact on other nodes. **(C)** With sinusoidal gain modulation at 29 Hz, two oscillators (natural frequencies 11.1 Hz and 47.0 Hz) selectively respond to the perturbation. **(D)** Average response amplitude (logarithm base 10) from t = 0 to t = 1.5 s at each oscillator versus gain frequency f_S. Different choices of gain frequency support selective coupling between the perturbed oscillator (natural frequency 17.9 Hz) and other oscillators. Peaks in response amplitude occur at golden rhythms (yellow circles, vertical lines) or other frequencies (red X's). Minimum response set to 0 for each curve, and vertical scale bar indicates 1. **(E)** Average amplitude (black curve) and range (2.5% to 97.5% from 100 simulations, shaded region) of evoked responses versus noise level. The oscillator with frequency 17.9 Hz is directly perturbed, and sinusoidal gain modulation occurs with $f_S \approx$ 29.0 Hz. Oscillators at golden rhythms exhibit different behavior with perturbation (red) versus without perturbation (gray). Code to simulate this network and create this figure is available here.

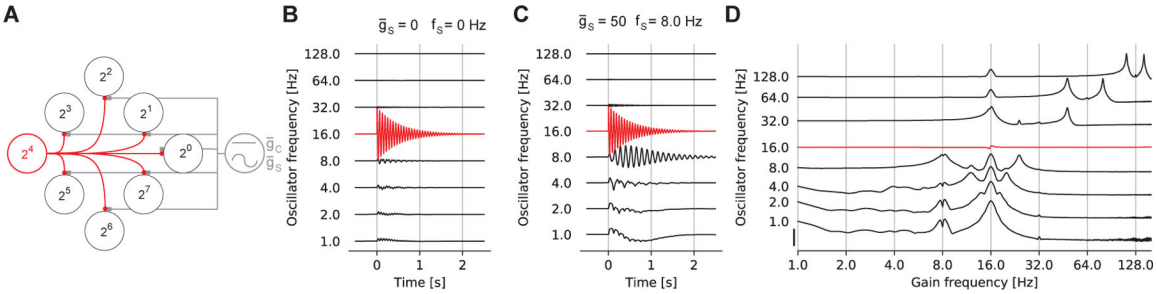

FIGURE 3. An integer scaling between oscillators limits cross-frequency interactions.

(A) In a network of oscillators with frequencies organized by a factor of 2, we perturb one oscillator (natural frequency 16 Hz, red). **(B)** With constant gain, the impact of the perturbation is limited. **(C)** With sinusoidal modulation at f_S = 8 Hz, a response appears at another oscillator (natural frequency 8 Hz). **(D)** The average response amplitude at each oscillator versus gain frequency f_S. Many oscillators respond when the gain frequency is 8 Hz, and responses tend not to occur at the oscillator frequencies; see Figure 2D for plot details. Code to simulate this network and create this figure is available here.

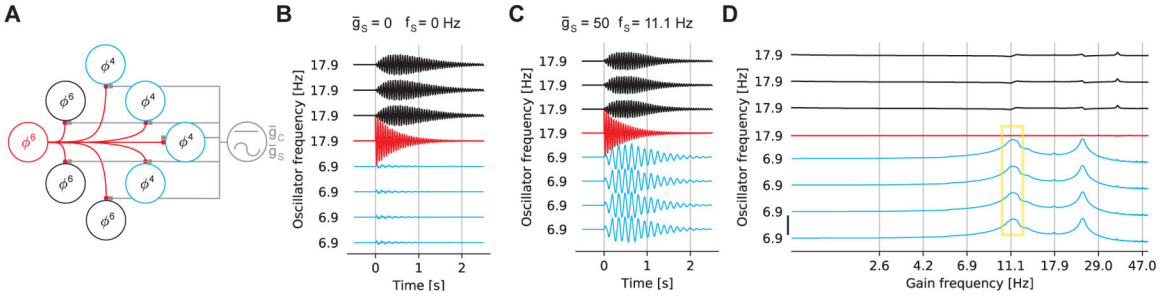

FIGURE 4. Golden rhythms support coupling among an ensemble of nodes.

(A) The network consists of two ensembles with frequencies: ϕ^4 and ϕ^6. **(B)** With constant gain, perturbing a node in one ensemble impacts (red) other nodes in the same ensemble (black). **(C)** With sinusoidal gain at frequency f_S = 11.1 Hz, the same perturbation impacts both ensembles. **(D)** Average amplitude response versus gain frequency for all nodes in both ensembles. The response at the unperturbed ensemble (blue) increases when the gain frequency is a golden rhythm (yellow box); see Figure 2D for additional plot details. Code to simulate this network and create this figure is available here.

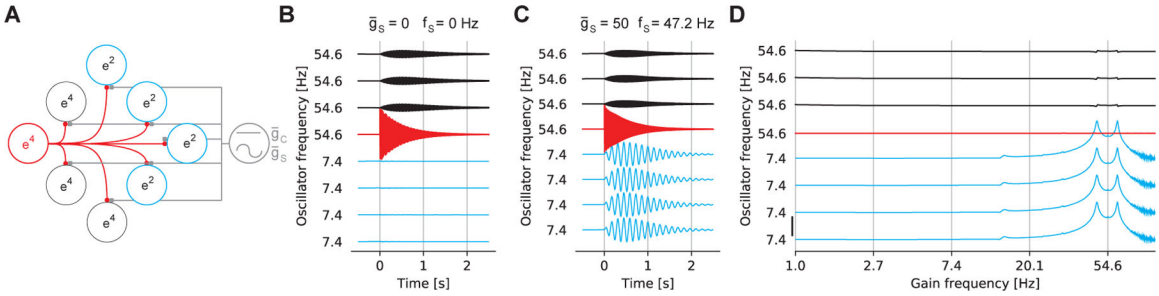

FIGURE 5. Rhythms organized by Euler's number do not support coupling between ensembles of nodes.

(A) The network consists of two ensembles with frequencies: e^4 and e^2. **(B)** With constant gain, perturbing a node in one ensemble impacts (red) other nodes in the same ensemble (black). **(C)** With sinusoidal gain at frequency $f_S = 47.2$ Hz, the same perturbation impacts both ensembles. **(D)** Average amplitude response versus gain frequency for all nodes in both ensembles. The response at the unperturbed ensemble (blue) does not increase when the gain frequency is a factor of the Euler number (black vertical lines); see Figure 2D for additional plot details. Code to simulate this network and create this figure is available here.

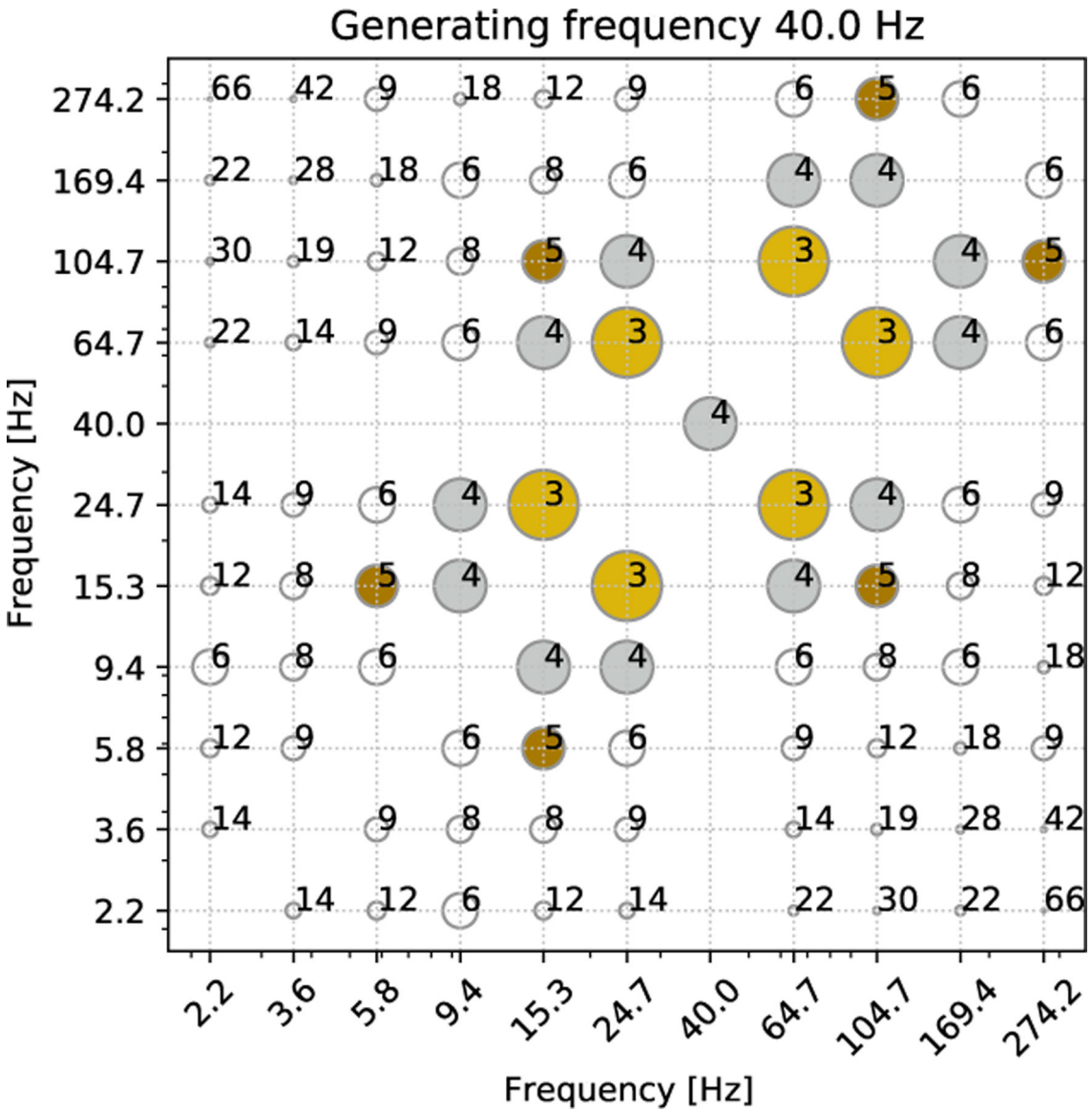

FIGURE 6. Golden rhythms establish triplets with a discrete set of resonance orders.
The resonance order (numerical value, marker size) for triplets generated from 40 Hz. Lower resonance orders (3,4,5) indicated in color (gold, silver, bronze, respectively). Code to simulate this network and create this figure is available here.

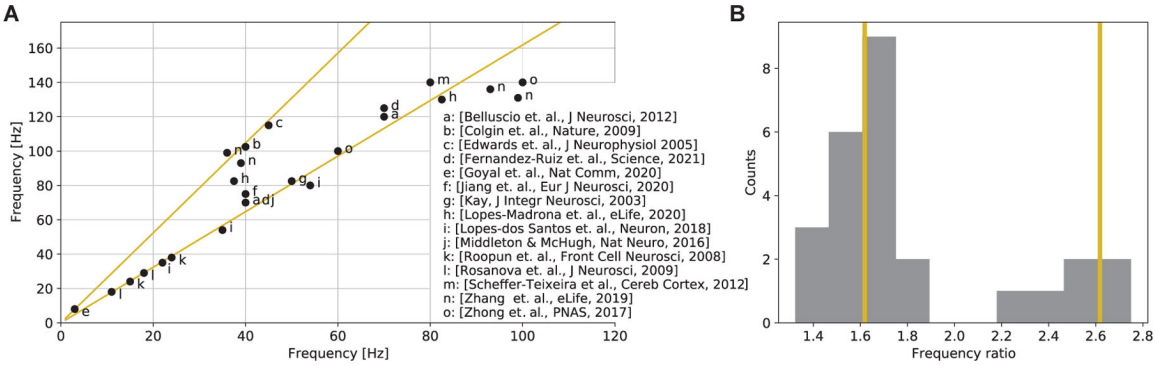

FIGURE 7. Empirical observations of rhythms organized by the golden ratio in vivo.

(A) Pairs of frequencies reported in the literature; see legend. When only a frequency band is reported, we select the mean frequency of the band. **(B)** Histogram of the frequency ratio for each point in (A). Lines (golden) indicate frequency bands organized by $\phi \approx 1.6$ or $\phi^2 \approx 2.6$. Code to create this figure is available here.

TABLE 1

Example sequence of golden rhythms.

Beginning with $f_{k+1} = 40$ Hz we compute the sequence of golden rhythms by multiplying or dividing by the golden ratio.

f_{k-5}	f_{k-4}	f_{k-3}	f_{k-2}	f_{k-1}	f_k	f_{k+1}	f_{k+2}	f_{k+3}	f_{k+4}	f_{k+5}
2.2	3.6	5.8	9.4	15.3	24.7	40	64.7	104.7	169.4	274.2

TABLE 2

Golden rhythms, beginning with the sidereal period, align with the brain's rhythms.

The period (T) and frequency (f) of rhythms beginning with the sidereal period (T = 86160 s) and multiplying the frequency by the golden ratio (number of multiplications indicated by the value in column **Power**). Traditional frequency band labels (from [37, 38, 42]) indicated in the last column.

Power	*T* [s]	*f* [Hz]	Power	*T* [s]	*f* [Hz]	Power	*T* [s]	*f* [Hz]	Label
0	86160	1.16E-05	12	268	0.004	24	0.83	1.20	Slow 1
1	53250	1.88E-05	13	165	0.006	25	0.51	2	Delta
2	32910	3.04E-05	14	102	0.010	26	0.32	3	Delta
3	20340	4.92E-05	15	63.2	0.016	27	0.20	5	Theta
4	12571	7.96E-05	16	39.0	0.026	28	0.12	8	Alpha
5	7769	1.29E-04	17	24.1	0.041	29	0.07	13	Beta1
6	4802	2.08E-04	18	14.9	0.067	30	0.05	22	Beta2
7	2968	3.37E-04	19	9.2	0.11	31	0.03	35	Low Gamma
8	1834	5.45E-04	20	5.7	0.18	32	0.02	57	Mid Gamma
9	1133	8.82E-04	21	3.5	0.28	33	0.01	91	High Gamma
10	701	0.001	22	2.2	0.46	34	0.01	148	Ripple
11	433	0.002	23	1.3	0.74	35	0.004	239	Fast Ripples